Conformational Phase Diagram for Polymers Adsorbed on Ultrathin Nanowires

Thomas Vogel[*] and Michael Bachmann[†]

*Soft Matter Systems Research Group, Institut für Festkörperforschung (IFF-2),
Forschungszentrum Jülich, D-52425 Jülich, Germany*

We study the conformational behavior of a polymer adsorbed at an attractive stringlike nanowire and construct the complete structural phase diagram in dependence of the binding strength and effective thickness of the nanowire. For this purpose, Monte Carlo optimization techniques are employed to identify lowest-energy structures for a coarse-grained model of a polymer in contact with the nanowire. Among the representative conformations in the different phases are, for example, compact droplets attached to the wire and also nanotubelike monolayer films wrapping it in a very ordered way. We here systematically analyze low-energy shapes and structural order parameters to elucidate the transitions between the structural phases.

PACS numbers: 82.35.Gh, 05.10.Ln, 61.48.De

Scrutinizing basic structural mechanisms of molecular binding at interfaces is crucial for a large field of interdisciplinary research and for potential applications. In recent years, there has been substantial progress in understanding general properties of polymer adhesion at solid substrates. This includes, for example, the identification of generic structural phases and the transitions between these [1–9], as well as specific binding affinities of proteins regarding the type of the substrate and the amino acid sequence [6,10–12]. In most of these studies, the substrate is considered as being planar. The influence of curved substrates on the formation of structural phases has been subject of works on droplet and helix formation at cylinders [13,14].

In this Letter, we systematically study conformational phases induced by an attractive nanowire, i.e., a substrate with one-dimensional topology. A nanowire could be, for example, a stretched polymer with the ends attached to dielectric beads fixed by optical tweezers. It is one of the most striking results of our study that for different parameter values of the polymer-nanowire interaction, i.e., in the corresponding region of the conformational phase diagram, the polymer crystallizes in stable cylindrical shapes with monomer alignments which resemble atomic arrangements known from single-walled carbon nanotubes. In this conformational phase, the cylindrical hull surrounds the thin wire such that the interior is free of particles. In a hydrodynamic application, for example, molecules could still flow through it. Since the axis of a polymeric tube is always oriented parallel to the direction of the wire, the growth direction of the tube can be controlled. This would enable the construction of complex tube systems and, therefore, allows for applications beyond those known for conventional nanotubes. Another conceivable application of this structural coincidence is the *systematic* stabilization or functionalization of nanotubes by polymer coating [15–17].

In our study, we investigate a coarse-grained model for the polymer and a stringlike substrate representing the nanowire. For the polymer, we employ a linear bead-stick model; i.e., covalent bonds between the N monomers are stiff. The chain is not grafted to the string and may move freely. The total energy of the system includes three contributions, $E = E_{\text{LJ}} + E_{\text{bend}} + E_{\text{string}}$. The interaction between nonadjacent monomers is governed by the standard Lennard-Jones (LJ) potential,

$$E_{\text{LJ}}(\{r_{ij}\}) = 4\epsilon_m \sum_{i=1}^{N-2} \sum_{j=i+2}^{N} \left[\left(\frac{\sigma_m}{r_{ij}}\right)^{12} - \left(\frac{\sigma_m}{r_{ij}}\right)^{6} \right], \quad (1)$$

with the distance r_{ij} between nonbonded monomers i and j. The monomer-monomer interaction parameters ϵ_m and σ_m are set to unity in the following. The weak bending energy is a remnant of the proteinlike origin of the model [18] and reads $E_{\text{bend}}(\{\cos\theta_i\}) = \kappa \sum_{i=2}^{N-1}(1 - \cos\theta_i)$ with the bending stiffness set to $\kappa = 1/4$. The bending angle θ_i is defined by the covalent bonds connected to the ith monomer. The monomer-string energy is obtained by continuously integrating a standard LJ potential over the infinitely long string [19]. We find

$$E_{\text{string}}(\{r_{\perp;i}\}) = \pi a \epsilon_f \sum_{i=1}^{N} \left(\frac{63}{64} \frac{\sigma_f^{12}}{r_{\perp;i}^{11}} - \frac{3}{2} \frac{\sigma_f^{6}}{r_{\perp;i}^{5}} \right), \quad (2)$$

where σ_f and ϵ_f are the monomer-string interaction parameters. The distance of the ith monomer perpendicular to the string is denoted by $r_{\perp;i}$. For convenience, we scale the potential such that its minimum is -1 at $r_\perp^{\text{min}}$ for $\epsilon_f = 1$ and $\sigma_f = 1$, in which case $a \approx 0.528$. The effective thickness of the string, σ_f, is related to the minimum distance $r_\perp^{\text{min}}$ of the monomer-string potential via $r_\perp^{\text{min}}(\sigma_f) = (693/480)^{1/6}\sigma_f \approx 1.06\sigma_f$. Alternatively, the monomer-string energy can be considered as the limiting case of the interaction of a monomer with a cylinder of radius $R \to 0$, keeping the overall LJ "charge" fixed [19].

We now systematically analyze the conformational phases of a polymer with $N = 100$ monomers for different
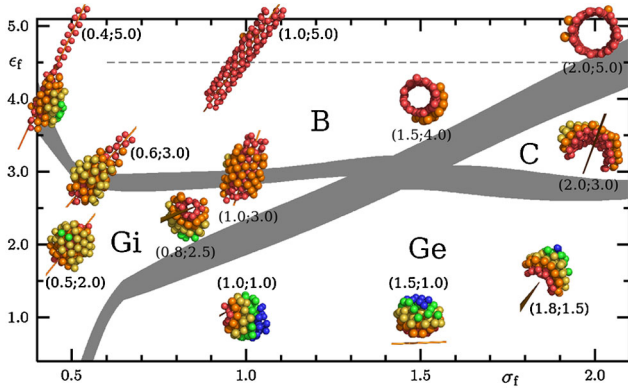
FIG. 1 (color online). The conformational phase diagram parametrized by the monomer-string potential parameters; from left to right, the effective string thickness σ_f increases and from bottom to top, the string attraction strength ϵ_f gets larger. Gray bands (widths correspond to uncertainty) indicate transition lines between compact, crystalline polymer structures with the string inclosed (Gi) or excluded (Ge), crescent-shaped (C), and barrel-like (B) conformations. The dashed line indicates a topological crossover that separates mono- and multilayer regions. Inset pictures show representative low-energy states. Monomers with the same coloring (or shadings) belong to the same layer.

values of effective thickness and attraction strength of the string, σ_f and ϵ_f, respectively. By "phase" we denote a domain in the parameter space, where the corresponding conformations share qualitatively the same morphology. In Fig. 1, the conformational phase diagram is shown and representative adsorbed polymer structures are depicted. This phase diagram is a result of extensive analyses of structural properties for more than 150 low-energy conformations with different values of interaction parameters. For the identification of lowest-energy conformations, we employed stochastic generalized-ensemble Monte Carlo methods such as multicanonical sampling [20], the Wang-Landau method [21], and energy-landscape paving optimization [22] which for this purpose performed equally well. Because of the energetic random-walk-like sampling of these methods, also the entropically highly suppressed low-energy conformations are accessible within a single simulation. For each parameter set, we generated up to 10^{11} updates, including local crankshaft, slithering-snake, global spherical cap, and translation moves [19]. The lowest-energy states identified in this way were subsequently refined by means of deterministic conjugate-gradient optimization. Repeating exemplified simulations in the different phases also for other chain lengths ($N = 30$ and $N = 200$), we find the same qualitative results as for the 100mer.

In the phase diagram, four major structural phases can be identified. For weak attraction ($\epsilon_f \lesssim 3$), two types of crystalline droplets [23] adhered to the string (regions Ge, Gi) can clearly be distinguished. Either the string axis is inclosed inside the droplet (Gi) or passes by externally

(Ge). If the adhesion strength of the string ϵ_f increases, compact droplets in Gi melt near $\epsilon_f \approx 3$ and phase B is entered, where polymer conformations extend along the string axis. Near $\epsilon_f \approx 4.5$, a crossover (dashed line in Fig. 1) from the multilayer barrel structures to monolayer conformations with strong similarities to single-walled nanotubes occur. According to former studies of polymer adsorption at planar substrates [4,9], this crossover corresponds to a topological transition between three-dimensional compact crystalline and two-dimensional filmlike structures. For sufficiently large values of the effective string thickness σ_f, the polymer layers do not completely wrap the tube and stable crescent-shaped "clamshell-like" [13] structures dominate in the region denoted by C.

Let us now have a closer look at the different conformational transitions. In region Gi, compact spherical conformations dominate. Increasing in this regime the attraction strength ϵ_f while keeping the effective thickness σ_f fixed, conformations lose their spherical shape at $\epsilon_f \approx 3$ and the cylindrical phase B is entered. This transition can be best characterized by introducing an asymmetry parameter based on the gyration tensor components parallel and perpendicular to the string, $A = r_\parallel^{\text{gyr}}/r_\perp^{\text{gyr}} - 1$. This order parameter is shown as a function of ϵ_f in Fig. 2, exemplified for $\sigma_f = 0.5$. In the spherical regime Gi, $A \approx 0$. As expected, A increases for $\epsilon_f \gtrsim 3$ and the structures become asymmetric. At this point, it is equally favorable for a monomer to stick to the string, or to form contacts to neighboring monomer layers. The conformations stretch along the string until they form a maximally compact monolayer tube surrounding the string for $\epsilon_f \gtrsim 4.5$.

Increasing, on the other hand, the effective thickness σ_f for values of the attraction strength $\epsilon_f < 3$, the transition from Gi to Ge is characterized by the different locations of the string relative to the droplet: it is inclosed (Gi) or excluded (Ge). For small values of ϵ_f, the transition point can be estimated as a first approximation by assuming a tetrahedral monomer-packing in the crystalline droplet. Then, the circumsphere radius of a tetrahedron is $r_\circ \approx 0.61$ which corresponds to a limiting effective string thickness $\sigma_{f,\circ} \approx 0.58$. Thus, inserting a string with $\sigma_f < \sigma_{f,\circ}$ does not break intramonomer contacts within a compact structure. Above this limiting value, however, the string would cause an energetically disfavored replacement of monomers inside the conformation and is hence "pushed" out of the droplet.

Quantitatively, this transition can be identified by measuring the opening angle α of a given conformation. Projecting the positions of monomers in contact with the string onto a plane perpendicular to the string, α is defined as the angle between the string and two monomers that spans the largest region of the plane with no monomers residing in. Thus, roughly, conformations with $\alpha < \pi$
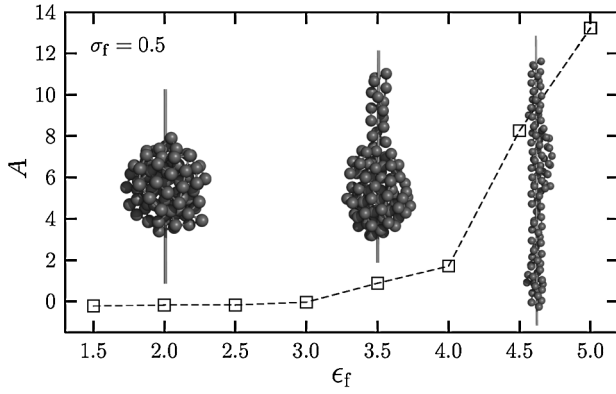
FIG. 2.   Asymmetry parameter A at small effective string thickness ($\sigma_f = 0.5$). The inset pictures show corresponding conformations at $\epsilon_f = 2.0$, 3.5, and 4.5, illustrating the transition from spherical to cylindrical low-energy structures. The conformational transition between Gi and B occurs near $\epsilon_f = 3.0$. For larger values of ϵ_f, A starts to significantly deviate from zero and conformations become cylindrical.

correspond to conformations inclosing the string (Gi), whereas $\alpha > \pi$, if the string is located outside the droplet (Ge). Figure 3 shows how α changes when crossing the transition line $Gi \leftrightarrow Ge$ horizontally or vertically. Fixing the attraction strength at $\epsilon_f = 3/2$, α increases rapidly from $\sigma_f \approx 0.65$ (squares, lower scale), which is close to the estimate $\sigma_{f,\circ}$ given above. For larger values of the effective thickness the string is shifted outwards to retain optimal monomer packing. The inset pictures show lowest-energy conformations at $\epsilon_f = 3/2$ and $\sigma_f = 1/2$ (representative for phase Gi) and $\sigma_f = 4/5$ (Ge), respectively. Increasing, on the other hand, the string attraction strength ϵ_f while $\sigma_f = 5/6$ is fixed (circles, upper scale), the inclusion of the string, accompanied by a rapid decrease of α, occurs at $\epsilon_f \approx 1.75$.

Starting in Ge and increasing σ_f and ϵ_f above certain threshold values results in the transition towards adsorbed curved conformations (C) in the sense that the polymer begins to wrap the string. Different monomer layers form. We quantitatively define this transition to occur at the point, where the distance of the center of mass of the polymer from the string, $r_\perp^{com} = N^{-1} | \sum_{i=1}^{N} \vec{r}_{\perp,i} |$, equals the monomer-string potential minimum distance $r_\perp^{min} (\approx 1.06 \sigma_f)$, i.e., at $\Delta r = r_\perp^{com} - r_\perp^{min} = 0$. Qualitatively, the center of mass intrudes into the virtual cylinder with radius $r_\perp^{min}$, defined by the inner layer of monomers. In Fig. 4, Δr is plotted as a function of ϵ_f at $\sigma_f = 7/3$. The transition point $\Delta r = 0$ is marked by the dotted line which is here intersected at $\epsilon_f = 2.9$, in correspondence to the $Ge \leftrightarrow C$ transition line in the phase diagram in Fig. 1. The shown inset pictures represent conformations with $\Delta r = 0.6$, -0.1, -0.8 at $\epsilon_f = 2, 3, 4$.

Finally, increasing ϵ_f further, region B is entered, i.e., ground-state polymer conformations wrap the string completely. If the attraction between a monomer and the string becomes stronger than the interaction between stacked, neighboring monomer layers, regular monolayer films surrounding the string are formed, i.e., single-walled tubes with an ordered arrangement of monomers. It is noticeable that there is a competition between different chiral orientations of the wrapping in dependence of the monomer-string interaction length scale σ_f [19]. This behavior is in a similar manner known from carbon nanotubes [24]. Defining the wrapping vector $\vec{c} = n\vec{a}_1 + m\vec{a}_2$, with $\vec{a}_1$ and $\vec{a}_2$ being the unit vectors of the structure, we even find the limiting "armchair" and "zigzag" structures, corresponding to $m = n$ and $m = 0$. Examples of nanotubelike polymer conformations with different chiralities are shown for $\sigma_f = 1.50, 1.57$ in Figs. 5(a) and 5(b),
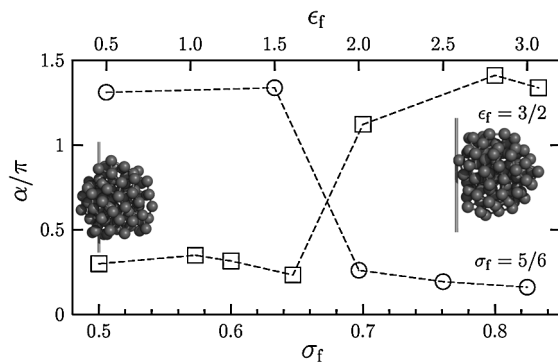

FIG. 3.   The plot shows the opening angle α of low-energy conformations for $\epsilon_f = 3/2$ in dependence of σ_f (squares, lower scale) and for $\sigma_f = 5/6$ as a function of ϵ_f (circles, upper scale). The inset pictures show corresponding conformations at $\epsilon_f = 3/2$ and $\sigma_f = 1/2, 4/5$, illustrating the separation of the droplet from the string.
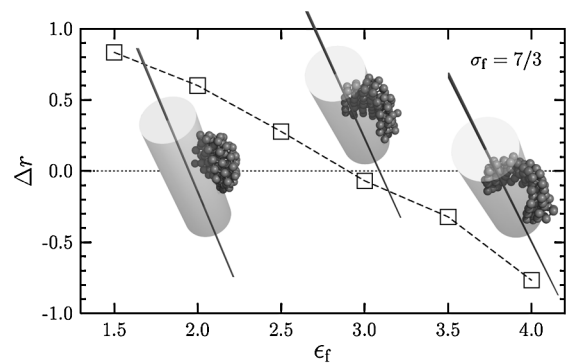

FIG. 4.   Distance Δr of the center of mass of the polymer from the virtual surface of the cylinder with the radius that corresponds to the minimum position of the string potential ($r_\perp^{min} \approx 1.06 \sigma_f$) for $\sigma_f = 7/3$. The intersection of the curve with the dotted line ($\Delta r = 0$) at $\epsilon_f = 2.9$, where the center of mass equals the radius of this cylinder, defines the transition from Ge to C. Pictures show conformations at $\epsilon_f = 2, 3,$ and 4.
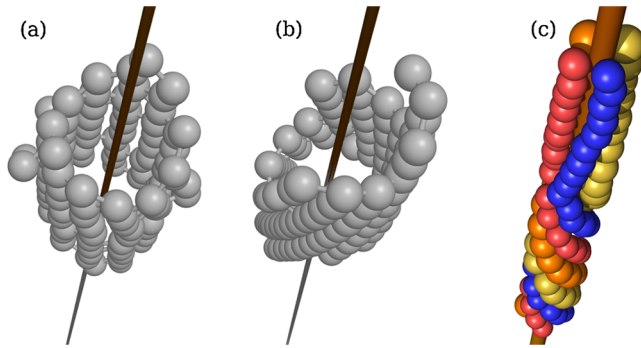
FIG. 5 (color online). Highly ordered cylindrical monolayer conformations of adsorbed polymers with different wrappings in the barrel phase B at $\epsilon_f = 5$ for (a) $\sigma_f = 1.50$, (b) $\sigma_f = 1.57$, and (c) $\sigma_f = 0.65$ (different colors or shadings shall facilitate the perception only). Geometric properties of these structures resemble chiral alignments of atomic structures known from single-walled nanotubes.

respectively, and for $\sigma_f = 0.65$ in Fig. 5(c) (all at $\epsilon_f = 5$). The alignment of monomers in Fig. 5(a) is almost parallel to the string, whereas the conformation in Fig. 5(b) exhibits a noticeable chiral winding. If the radius of the monolayer polymer tube does not allow for a perfect monomer alignment, defects occur and cause the formation of structural domains with different chiralities within the same conformation [19], as in the example shown in Fig. 5(c).

To summarize, we have constructed the entire conformational phase diagram for a system consisting of a flexible polymer and an ultrathin attractive nanowire in dependence of the energy scales and length scales associated to the polymer-nanowire interaction. We identified conformational phases of compact spherical polymer droplets inclosing or excluding the string, and a phase of compact but curved shapes (crescent-shaped structures). For sufficiently large string attraction strengths, we observe the formation of cylindrical conformations which in the extreme case of monolayer structures possess strong similarities to nanotubes. This is particularly interesting as it shows that polymers can form tubelike structures in a controlled way. Since the polymer tube can adapt any orientation of the guiding nanowire, also the formation of complex, nonlinear tube systems with bends is conceivable. This would enable a wide range of potential applications which are hard to construct by atomic nanotubes.

*t.vogel@fz-juelich.de
†m.bachmann@fz-juelich.de; http://www.smsyslab.org

[1] T. Vrbová and S. G. Whittington, J. Phys. A **29,** 6253 (1996); **31,** 3989 (1998).
[2] A. Milchev and K. Binder, J. Chem. Phys. **114,** 8610 (2001).
[3] R. Rajesh, D. Dhar, D. Giri, S. Kumar, and Y. Singh, Phys. Rev. E **65,** 056124 (2002).
[4] M. Bachmann and W. Janke, Phys. Rev. Lett. **95,** 058102 (2005); Phys. Rev. E **73,** 041802 (2006).
[5] J. Krawczyk, T. Prellberg, A. L. Owczarek, and A. Rechnitzer, Europhys. Lett. **70,** 726 (2005).
[6] M. Bachmann and W. Janke, Phys. Rev. E **73,** 020901(R) (2006).
[7] N. Källrot and P. Linse, Macromolecules **40,** 4669 (2007).
[8] J. Luettmer-Strathmann, F. Rampf, W. Paul, and K. Binder, J. Chem. Phys. **128,** 064903 (2008).
[9] M. Möddel, M. Bachmann, and W. Janke, J. Phys. Chem. B **113,** 3314 (2009).
[10] S. R. Whaley, D. S. English, E. L. Hu, P. F. Barbara, and A. M. Belcher, Nature (London) **405,** 665 (2000).
[11] M. Sarikaya, C. Tamerler, A. K.-Y. Jen, K. Schulten, and F. Baneyx, Nature Mater. **2,** 577 (2003).
[12] K. Goede, P. Busch, and M. Grundmann, Nano Lett. **4,** 2115 (2004); K. Goede, M. Grundmann, K. Holland-Nell, and A. G. Beck-Sickinger, Langmuir **22,** 8104 (2006).
[13] A. Milchev and K. Binder, J. Chem. Phys. **117,** 6852 (2002).
[14] I. Gurevitch and S. Srebnik, Chem. Phys. Lett. **444,** 96 (2007); J. Chem. Phys. **128,** 144901 (2008); S. Srebnik, J. Polym. Sci., Part B: Polym. Phys. **46,** 2711 (2008).
[15] M. Gao, L. Dai, and G. G. Wallace, Electroanalysis **15,** 1089 (2003); T. Hasan, Z. Sun, F. Wang, F. Bonaccorso, P. H. Tan, A. G. Rozhin, and A. C. Ferrari, Adv. Mater. **21,** 3874 (2009).
[16] L. Valentini, J. Biagiotti, J. M. Kenny, and S. Santucci, J. Appl. Polym. Sci. **87,** 708 (2003); L. Valentini, J. Biagiotti, M. A. López-Manchado, S. Santucci, and J. M. Kenny, Polym. Eng. Sci. **44,** 303 (2004).
[17] A. Sorkin, J. Adler, and R. Kalish, Phys. Rev. B **78,** 155435 (2008).
[18] F. H. Stillinger, T. Head-Gordon, and C. L. Hirshfeld, Phys. Rev. E **48,** 1469 (1993).
[19] T. Vogel and M. Bachmann (to be published).
[20] B. A. Berg and T. Neuhaus, Phys. Lett. B **267,** 249 (1991); Phys. Rev. Lett. **68,** 9 (1992).
[21] F. Wang and D. P. Landau, Phys. Rev. Lett. **86,** 2050 (2001).
[22] U. H. E. Hansmann and L. T. Wille, Phys. Rev. Lett. **88,** 068105 (2002).
[23] T. Vogel, M. Bachmann, and W. Janke, Phys. Rev. E **76,** 061803 (2007); S. Schnabel, T. Vogel, M. Bachmann, and W. Janke, Chem. Phys. Lett. **476,** 201 (2009).
[24] J. W. G. Wilder, L. C. Venema, A. G. Rinzler, R. E. Smalley, and C. Dekker, Nature (London) **391,** 59 (1998); T. W. Odom, J.-L. Huang, P. Kim, and C. M. Lieber, *ibid.* **391,** 62 (1998).